OPEN BIOLOGY

royalsocietypublishing.org/journal/rsob

Research

Cite this article: Santalla M, Sonda S, Bertocco A, Ciocci Pardo A, Greotti E, Pendin D. 2026 FRET-based fluorescent sensors for cytosolic and mitochondrial Ca^{2+} imaging in *Drosophila melanogaster*. *Open Biol.* **15**: 250197. https://doi.org/10.1098/rsob.250197

Received: 5 June 2025
Accepted: 13 November 2025

Subject Areas:
cellular biology, neuroscience, genetics

Keywords:
Drosophila melanogaster, genetically encoded Ca^{2+} indicators, mitochondria, FRET, calcium

Authors for correspondence:
Elisa Greotti
e-mail: elisa.greotti@cnr.it
Diana Pendin
e-mail: diana.pendin@cnr.it

Electronic supplementary material is available online at https://doi.org/10.6084/m9.figshare.c.8254418.

THE ROYAL SOCIETY PUBLISHING

FRET-based fluorescent sensors for cytosolic and mitochondrial Ca^{2+} imaging in *Drosophila melanogaster*

Manuela Santalla[1,2], Sonia Sonda[1,2], Ambra Bertocco[2], Alejandro Ciocci Pardo[2], Elisa Greotti[1,2,3] and Diana Pendin[1,2]

[1]Neuroscience Institute, National Research Council, Padua, Italy
[2]Department of Biomedical Sciences, and [3]Padova Neuroscience Centre (PNC), University of Padua, Padua, Italy

MS, 0000-0002-3590-9586; SS, 0000-0002-7972-8728; AB, 0000-0002-8018-6989; ACP, 0000-0002-2832-685X; EG, 0000-0003-3702-4789; DP, 0000-0003-2827-935X

Ca^{2+} imaging in the living tissues of experimental animals currently presents limitations due to motion artefacts, variable expression levels and the low basal fluorescence of available probes. These issues are even more troublesome when performing Ca^{2+} imaging in contractile tissues and moving organelles. Despite the well-known advantages of ratiometric sensors, their application in experimental animals is still limited. This study addresses these challenges in the fruit fly *Drosophila melanogaster*, introducing the development and characterization of novel transgenic fly lines expressing advanced FRET-based Cameleon probes for cytosolic and mitochondrial Ca^{2+} imaging. A series of Ca^{2+} imaging experiments in selected tissues demonstrates their functionality. These newly developed tools guarantee precise and quantitative measurement of Ca^{2+} in various cellular contexts, which will contribute to advancing Ca^{2+} research in *Drosophila*.

1. Background

Cellular physiology strictly relies on calcium (Ca^{2+}) signalling. Since the first prototypes of Ca^{2+} indicators were developed, tremendous advances have been made in understanding the complex pathways governing cell physiology and pathology. Despite these successes, certain areas of Ca^{2+} imaging, particularly those aimed at investigating organelle Ca^{2+} handling in the living tissues of experimental animals, are still underdeveloped and require further efforts to construct robust imaging tools.

Drosophila melanogaster is among the most commonly used model organisms in scientific research. The lack of genetic redundancy and the availability of an annotated genome since 2000 have consolidated robust molecular and genetic techniques. In addition to its genetic accessibility, the fruit fly's complex behavioural repertoire and its functional similarities to mammals make it an attractive model organism for addressing relevant physiological and pathological questions at the cellular, organ and even whole organism levels.

For the Ca^{2+} research community, *Drosophila* offers the advantages of a conserved Ca^{2+} molecular toolkit, making the fruit fly an interesting model for Ca^{2+} research. Over the past two decades, fly lines expressing Ca^{2+} indicators have been developed, and Ca^{2+} imaging procedures tailored for each stage of fly development have been devised. While a series of single-wavelength indicators have been developed, and fly lines have been generated for their expression [1,2], they often exhibit no fluorescence at basal Ca^{2+} levels and are prone to pH artefacts. Therefore, the use of an internal normalizer, such

as fusion with a red fluorescent protein (FP), is mandatory to permit pseudo-ratiometric measurements (e.g. [3]).

It is widely accepted that a ratiometric sensor is the preferred choice when dealing with animal tissues due to its independence from motion artefacts, particularly relevant when imaging live tissues and probe expression levels. Moreover, ratiometric imaging allows a quantitative estimation of Ca^{2+} concentration ($[Ca^{2+}]$). The most commonly used ratiometric sensors are based on Förster resonance energy transfer (FRET), where Ca^{2+} binding induces changes in FRET efficiency between two FPs. *Drosophila* lines expressing FRET-based probes have been reported using Cameleons based on the classical Enhanced Cyan Fluorescent Protein (ECFP)/Enhanced Yellow Fluorescent Protein (EYFP) couple [4–6]. Flies expressing Cameleon probes in the nervous system did not show evident phenotypic changes or alterations in electrophysiological recordings compared to wild-type flies [6], indicating that the sensor is well tolerated when expressed in the cytosol.

Ca^{2+} sensors have been targeted to the mitochondrial matrix in *Drosophila*; however, these sensors are mostly single-wavelength [7–12]. This implies that imaging results are susceptible to interference from tissue and organelle motion artefacts and are plagued by low basal fluorescence. Even more than during Ca^{2+} imaging experiments in the cytosol, in mitochondrial matrix Ca^{2+} investigations using single-wavelength sensors, the co-expression of a red FP is necessary to serve as a normalizer for expression level and movement artefacts. However, this strategy requires a second UAS-construct, thus complicating the genetics of crossings when expressing a transgene of interest.

The use of ratiometric sensors would overcome these limitations; however, only a few transgenic fly lines have been generated so far [13,14]. In a rigorous study aimed at investigating the effect of mitochondrial matrix free Ca^{2+} level on motor neuron energy metabolism, Ivannikov and Macleod developed transgenic fly lines for the expression of high-affinity mito-D4cpv and low-affinity mito-TN-XXL, two ratiometric sensors targeted to the mitochondrial matrix [13]. Leveraging the distinct affinities for Ca^{2+} of the two probes, the authors estimated the mitochondrial matrix $[Ca^{2+}]$ in motor neuron presynaptic terminals at rest (approx. 0.22 µM, measured with mito-TN-XXL) and during nerve stimulation (approx. 27 µM upon 42 Hz stimulation, measured with mito-D4cpv). Despite the obvious advantages of precise, quantitative measurements of matrix Ca^{2+}, no other ratiometric sensors have been developed subsequently.

We thus decided to broaden the repertoire of available fly lines for the expression of ratiometric probes designed for cytosolic and mitochondrial Ca^{2+} imaging. Among the options, we selected the FRET, mCerulean3-based Cameleon probes D3mC3+16 and 4mtD3mC3+16 [15], improved versions of classical ECFP/Circularly Permuted Venus (cpV) couple-based Cameleon probes with enhanced photophysical properties that allow their usage in both intensity- and lifetime-based approaches. Here, we describe the generation and characterization of two novel transgenic fly lines for the expression of cytosolic D3mC3+16 and mitochondria-targeted 4mtD3mC3+16 Cameleon sensors. The probe sequences were placed under the control of UAS, allowing the generation of transgenic lines for the controlled expression of the sensors. These probes can be expressed in a tissue-specific and controlled manner upon a single genetic cross with a fly line carrying the transcription factor Gal4 downstream of a tissue-specific or temporally controlled promoter [16]. Finally, we provide a series of Ca^{2+} imaging experiments in isolated neurons, adult fly brains or hearts, demonstrating the functionality and versatility of the probes.

2. Methods

2.1. Molecular biology and line generation

D3mC3+16 and 4mtD3mC3+16 sequences were PCR-amplified using primers to insert a 5′ KpnI restriction site and a 3′ XhoI restriction site. pCDNA3-D3mC3+16 and pCDNA3-4mtD3mC3+16 [15] were used as templates, respectively. The sequences were cloned downstream of a UAS in the pUAST vector, resulting in pUAST-D3mC3+16 and 4mtD3mC3+16 constructs (electronic supplementary material). To generate UAS fly lines, the two plasmids were microinjected into w^{1118} embryos (BestGene Inc.), leading to the establishment of UAS-D3mC3/TM3 and UAS-4mtD3mC3/TM3 fly lines used in this study.

2.2. Fly stocks and husbandry

Flies were reared on a standard cornmeal yeast medium (DiBio Fly Facility, University of Padua). The following Gal4 lines were used to drive the expression of Cameleon probes in the indicated tissues: D42-Gal4 (motor neurons, BDSC 8816) and MHC-Gal4 (muscle, BDSC 38464). A line stably expressing 4mtD3mC3 under the control of the D42-GAL4 driver (UAS-4mtD3mC3, D42-Gal4/TM6) was generated by genetic recombination. The partial loss of the mitochondrial Ca^{2+} uniporter (MCU) was achieved by crossing UAS-4mtD3mC3, D42-GAL4/TM6 flies with MCU^{1} flies, kindly gifted by Alex Whitworth (University of Cambridge) [17]. UAS-4mtD3mC3, D42-GAL4/MCU^{1} flies were used for imaging experiments as $MCU^{+/-}$.

2.3. Tissue preparation and staining

Fly adult brains and muscles expressing either D3mC3+16 or 4mtD3mC3+16 were dissected in a haemolymph-like buffer (HL3) at room temperature. For cytosolic probe localization, tissues were mounted freshly and imaged.

For mitochondrial probe localization, after dissection, unfixed tissues were incubated for 30 min at 28°C with the mitochondrial marker MitoTracker Deep Red (1 µM) (Thermo Fisher Scientific, M22426) while protected from light. After washing twice in HL3, tissues were mounted in microscope glasses with HL3.

Samples were imaged on a Leica Stellaris 8 confocal microscope equipped with a 100× objective. Illumination was achieved by a white laser, and excitation/emission wavelengths were set at 515/525–550 nm and 649/666–700 nm for cpV and MitoTracker Deep Red, respectively. Images were analysed offline with ImageJ software.

2.4. Protein extraction and western blotting

Proteins were extracted from 6 fly bodies expressing D3mC3+16 or 4mtD3mC3+16 under the control of the MHC-Gal4 driver or from 20 fly heads expressing D3mC3+16 or 4mtD3mC3+16 under the control of the D42-Gal4 driver. Bodies or heads were placed in RIPA buffer (50 mM Tris, 150 mM NaCl, 1% Triton X-100, 0.5% deoxycholic acid, 0.1% SDS, protease and phosphatase inhibitor cocktails; Roche, 11836170001 and 4906845001, respectively, pH 7.5) and homogenized with a pestle, and then the lysates were incubated on ice for 30 min. The supernatants were collected after being spun down at 13 000 × *g* for 15 min at 4°C. Then, 20 µg of the proteins was separated by SDS-PAGE, transferred into PVDF membranes (Thermo Fisher Scientific, 88520) and probed using the following antibodies: anti-GFP (Cell Signalling, 2956, 1:5000); anti-actin (Sigma-Aldrich, A2066, 1:5000), Goat Anti-Rabbit IgG Antibody, F(ab')2, HRP conjugate (Sigma-Aldrich, AQ132P, 1:3000). Chemiluminescence was detected using a Mini HD9 chemidoc system (Uvitec Cambridge).

2.5. Cultured neuron imaging

The preparation of larval neurons was performed as previously described [18], with minor modifications. Briefly, third-instar larvae were collected in a Petri dish, rinsed once with double-distilled water, twice with 70% ethanol and then with the dissecting solution, consisting of Schneider's Insect Medium (Sigma-Aldrich, S9895) supplemented with 50 µg ml^{-1} insulin (Sigma-Aldrich, I6634) and antibiotic–antimycotic solution 1× (Sigma-Aldrich, A5955), pH 7.4 at 28°C. Brains were dissected with sterilized forceps under a light microscope. Brains were washed twice with the dissecting solution and then transferred to an enzyme solution containing 0.75 µg $µl^{-1}$ Collagenase, Type I (Gibco, 17018-029) and 0.4 µg $µl^{-1}$ dispase II (Roche, 04942078001) in dissecting solution. During incubation, brains were mechanically dissociated by gentle pipetting. The resulting cell lysates were centrifuged at 500 × *g* for 5 min and washed twice with Schneider's Complete Medium (dissecting solution supplemented with 10% FBS) to remove any residual enzymes. The cell pellet was resuspended in Schneider's Complete Medium. Then, 50 µl of cell suspension, approximately corresponding to two brains, was drop-plated for each 18-mm round coverslip in a 12-well plate. Coverslips were previously autoclaved and coated with 15 µg ml^{-1} Concanavalin A (Sigma-Aldrich, C2010) for 2 h at room temperature. The plate was stored in a humidified container at 28°C until the day of the experiment.

Larval neurons expressing Cameleon probes, cultured 4–5 days *in vitro*, were imaged on an inverted microscope (Nikon Ti-E) with a 40× oil objective (S Fluor, NA 1.30). Fluorescence illumination was provided by a 75 W lamp (USHIO UXLS50A), and the excitation wavelength (427 ± 5 nm) was obtained by a monochromator (Optoscan CAIRN-Research) controlled by NIS-Elements AR (Nikon) software. The excitation light was further refined by passing through a bandpass filter (438/24, Semrock) and a dichroic mirror (FF458-Di02, Semrock). The emitted light was collected through a beam splitter, equipped with emission filters FF01-479/40 (Semrock) for mCerulean3 and FF01-542/27 (Semrock) for cpV; dichroic mirror T515LPXR-UF2 (Chroma). Images were acquired every second, with an exposure time of 80–100 ms for each wavelength, using a Zyla-CMOS 4.2 P (Andor, Oxford Instruments) controlled by NIS-Elements AR (Nikon) software.

During the experiment, cells plated on coverslips were mounted into an open-topped chamber and maintained in an extracellular-like medium containing 30 mM HEPES, 150 mM NaCl, 2.8 mM KCl, 2 mM $MgCl_2$, 35 mM sucrose, 5 mM glucose and 1 mM $CaCl_2$ (pH 7.4 with NaOH) at room temperature, and 500 µM carbachol (Sigma-Aldrich C4382) was used to induce a cytosolic transient Ca^{2+} increase. At the end of the experiment, 10 µM ionomycin (Sigma-Aldrich, 407950) was added to achieve the maximum [Ca^{2+}].

2.6. Whole organ Ca^{2+} imaging

2.6.1. Brain imaging

Imaging experiments were performed using a naked brain preparation. Whole brains from flies of different ages were dissected in ice-cold, brain-specific HL3 [19] containing 5 mM HEPES, 10 mM $NaHCO_3$, 70 mM NaCl, 5 mM KCl, 1.5 mM $CaCl_2$, 20 mM $MgCl_2$, 5 mM trehalose and 115 mM sucrose (pH 7.1). After dissection, brains were placed on a 35 mm glass-bottom dish (glass diameter 12 mm) (Thermo Fisher Scientific), completely bathed in HL3 and allowed to recover for 3–5 min before the experiment.

Imaging experiments were performed using a Leica Thunder microscope with a 20× (NA = 0.8) immersion lens. The white LED in pE-340fura (CoolLED) was used as a light source; the filter cube was set as follows: Ex: 420/20; Dic: 455, 515 nm. The emitted light collection was obtained through CFP/YFP image splitting by a Hamamatsu W-VIEW GEMINI system equipped with FRET Filterset (CFP/YFP) as follows: Dic: 502; Em CFP: 480/40; Em YFP: 535/30 nm. Recordings were captured using a CCD camera (ORCA-Flash4.0 by Hamamatsu, C13440) at a frequency of 2 Hz with a 20 ms exposure and 2 × 2 binning. Baseline images were collected for 30–60 s before applying stimuli to the brain. 15 mM KCl or 5 µM ionomycin was used to induce Ca^{2+} transients.

2.6.2. Heart imaging

Flies were anaesthetized and held dorsally with vaseline in a 35 mm glass-bottom dish (glass diameter 12mm) (Thermo Fisher Scientific). Fly hearts were dissected in oxygenated, heart-specific HL3 [20]. Semi-intact heart preparation was performed as previously described [21], and isolated hearts were placed in a 35 mm Petri dish with a 21 mm polymer-coated observation area (μ-Dish 35 mm, high Glass-Bottom, ibidi GmbH) and submerged in HL3.

Heart preparations were imaged using a Leica Thunder microscope equipped as described above. Recordings were captured at a frequency of 66 Hz with 3 ms exposure and 2 × 2 binning. 5 μM ionomycin and 20 mM ethylene glycol-bis(β-aminoethyl ether)-*N*,*N*,*N*′,*N*′-tetraacetic acid (EGTA) (Sigma-Aldrich E4378) were used to induce maximal and minimal Ca^{2+} influx. 1 mg ml^{-1} 2,3-butanedione monoxime (BDM, Sigma-Aldrich 203984) was placed to inhibit cell contraction.

2.6.3. Ca^{2+} imaging analysis

Offline analysis of Ca^{2+} imaging experiments was performed using NIS-Elements software or Leica Application Suite X software. $F_{mCerulean3}$ and F_{cpV} images were subtracted from background signals, and regions of interest (ROIs) were selected on each imaged cell. The ratio of the emitted fluorescence intensities ($R = F_{acceptor}/F_{donor} = F_{cpV}/F_{mCerulean3}$) was calculated for each ROI, normalized to the value measured before stimulus addition (R_0, calculated as the average of at least 10 frames). Data were analysed using Microsoft Excel and GraphPad Prism 8.

2.6.4. Statistical analyses

The traces reported in the graphs are representative. All experiments were independently repeated at least three times. Average values are expressed as mean ± standard error of the mean (n = number of brains). Statistical analyses were performed using an unpaired Student's t-test, with a confidence interval of 95% (*$p < 0.05$, **$p < 0.01$, ***$p < 0.001$).

3. Results

3.1. Generation and characterization of mCerulean3-based Cameleon fly lines

In an effort to extend the repertoire of available strategies for ratiometric Ca^{2+} imaging in the fruit fly *Drosophila melanogaster*, we have developed two novel transgenic fly lines for the controlled expression of either a cytosolic or a mitochondria-targeted probe. The use of a FRET-based sensor guarantees ratiometric measurements, which are independent of sample movement and probe expression level. This becomes particularly relevant when measuring Ca^{2+} within mitochondria, highly dynamic organelles that move unceasingly, or naturally moving samples such as hearts. Although FRET-based Cameleon probes are valued for their robustness and extensive characterization, the only available fly line expressing a Cameleon sensor in the mitochondrial matrix is the mito-D4cpv line [13]. Recently, we generated an improved Cameleon version addressing the major limitations of the original family of probes—namely, the relatively low fluorescence quantum yield of the donor FP and the pH dependency of the probe. This probe is based on the D3 domain, which has a higher affinity for Ca^{2+} than the D4 domain. Notably, D3 has a single affinity for Ca^{2+} (K_d), which is suitable for measurements within both the mitochondrial matrix and the cytosol (K_d = 0.6 μM [22]). These ameliorated versions of Cameleon were obtained by(i) replacing the original ECFP donor with mCerulean3, a brighter and less pH-sensitive FP, and (ii) modifying the sequence to improve targeting efficiency and fluorescence changes caused by Ca^{2+} binding. Cytosolic and mitochondria-targeted versions of the probe, named D3mC3+16 and 4mtD3mC3+16, respectively, have been successfully employed to measure [Ca^{2+}] variations in isolated cells, as well as in mouse tissues *ex vivo* and *in vivo*, demonstrating their superiority over ECFP-based versions. Notably, the substantial increase in the signal-to-noise ratio observed in mCerulean3-based sensors makes them an ideal choice for imaging tissues in live animals. Despite this, mCerulean3-based Cameleon has not yet been used to generate transgenic animals.

The sequences of Cameleon probes, D3mC3+16 and 4mtD3mC3+16, were cloned into the pUAST vector under the control of the UAS sequence and microinjected into w^{1118} embryos to generate the two transgenic lines named UAS-D3mC3 and UAS-4mtD3mC3 (figure 1A). The UAS/Gal4 system [16] enables the expression of the probe in specific cell types by using selected promoters. While the expression of the cytosolic probe did not impact long-term fly survival, the mitochondria-targeted construct induced lethality at the larval stage when crossed with the ubiquitous drivers tubulin-Gal4 and daughterless (DA)-Gal4, as well as with the strong muscle-specific driver Mef2-Gal4. Nevertheless, the lethality was circumvented by using a weaker muscle-specific driver, such as MHC-Gal4 or the motor neuron-specific driver D42-Gal4. The two drivers ensured robust expression of both probes, as confirmed by western blot of fly tissues (figure 1B).

Probe localization was then tested in UAS-D3mC3/D42-Gal4 and UAS-D3mC3/MHC-Gal4, as well as in UAS-4mtD3mC3/D42-Gal4 and UAS-4mtD3mC3/MHC-Gal4 adult brain and muscle preparations. Colocalization with MitoTracker™ DeepRed signal confirmed the proper mitochondrial localization of 4mtD3mC3 (figure 1C), with no observable diffuse cytoplasmic staining. On the contrary, the D3mC3 signal appeared diffuse, consistent with the expected pattern for a cytosolic protein (figure 1D).

Finally, the ability of the probes to detect Ca^{2+} transients was then assessed across various experimental paradigms, ranging from isolated cells to whole-tissue preparations.

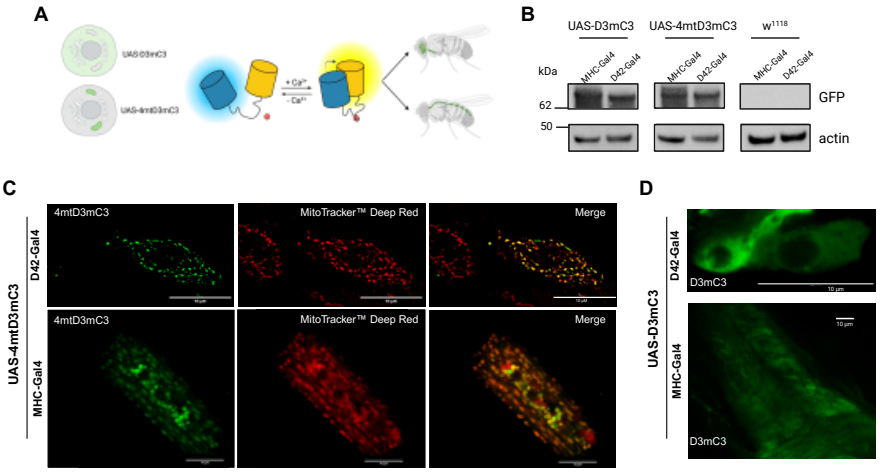

Figure 1. (A) Schematic representation of the generation of the new transgenic lines. (B) Expression of mCerulean3-based Cameleon probes in fly tissues as analysed by western blotting using an anti-GFP antibody. (C,D) Confocal images from motor neurons (top) and myocytes (bottom) expressing either D3mC3+16 or 4mtD3mC3+16 probes (green) and stained with the mitochondrial marker MitoTracker™ (red). Scale bar, 10 µm.

3.2. Ca^{2+} dynamics imaged by Cameleon probes in cultured neurons

Neurons were isolated from third-instar larvae expressing UAS-D3mC3 or UAS-4mtD3mC3 under the control of the motor neuron-specific driver D42-Gal4 (figure 2A). After 4–5 days in culture, motor neurons expressing D3mC3+16 were imaged. Following the recording of basal fluorescence, neurons were stimulated with the cholinomimetic drug carbachol to stimulate muscarinic receptors, inducing an increase in intracellular Ca^{2+} levels. As expected, upon stimulation, the acceptor fluorescent signal increased, while the donor fluorescent signal decreased, resulting in an increase in the calculated ratio ($R = F_{acceptor}/F_{donor}$) that mirrors the increase in cytosolic Ca^{2+} (figure 2B,C). Similar results were obtained when imaging neurons expressing 4mtD3mC3+16, demonstrating the capability of the sensor to measure Ca^{2+} changes also within the mitochondrial matrix. At the end of each experiment, a pulse of ionomycin in the presence of high [Ca^{2+}] was applied to reach maximal Ca^{2+} influx (figure 2D,E).

3.3. Ca^{2+} dynamics imaged by Cameleon probes in *Drosophila* brains

We subsequently tested the functionality of the probes in adult tissues. Whole brains were isolated from three-week-old flies expressing UAS-D3mC3 under the control of the motor neuron-specific driver D42-Gal4 (figure 3A). Isolated brains were imaged while maintained in a bath and challenged with KCl. As expected, KCl-induced depolarization led to an increase in the calculated *R*, indicative of the rise in cytosolic Ca^{2+} due to the opening of voltage-gated plasma membrane channels (figure 3B,C).

Similar results were obtained in brains expressing the mitochondria-targeted probe UAS-4mtD3mC3 during KCl stimulation (figure 3D,E). Importantly, treatment of the brain with carbonyl cyanide-4-(trifluoromethoxy)phenylhydrazone (FCCP), an ionophore that dissipates mitochondrial membrane potential, thereby nullifying the driving force for matrix Ca^{2+} entry, was sufficient to abolish the increase in *R* upon KCl stimulation (figure 3F). This further confirms the proper mitochondrial matrix localization of 4mtD3mC3 in flies.

Altogether, the collected data confirm the ability of the probes expressed in the two newly generated fly lines to measure Ca^{2+} changes in the cytosol or selectively in the mitochondria in the brain.

The ability of the 4mtD3mC3 probe to properly detect matrix [Ca^{2+}] change has been further tested in flies where the MCU, the channel responsible for mitochondrial Ca^{2+} uptake [23,24], was partially lost. Brains isolated from 4-day-old $MCU^{+/-}$ and control flies expressing UAS-4mtD3mC3 in motor neurons were challenged by applying KCl, and mitochondrial [Ca^{2+}] was monitored. As expected, $MCU^{+/-}$ exhibited decreased Ca^{2+} uptake, reflected by lower peak heights (figure 3G(i)) and uptake velocities (figure 3G(ii)) than controls. No changes were found in basal Ca^{2+} levels as measured before the stimulus (figure 3G(iii)).

Ca^{2+} signalling has been implicated in fundamental processes throughout development and ageing [25–29]. For this reason, it is important for a probe to retain its functionality across different stages of the animal's life. We tested the expression of mitochondrial and cytosolic Cameleon probes at two time points during the fly's life and their ability to respond to [Ca^{2+}] variations. Brains were dissected from flies aged 4 or 21 days and imaged as previously described. A depolarizing stimulus was perfused, and the resulting Ca^{2+} increase, as reported by the Cameleon probe, was evaluated (figure 4A,B). No differences were observed in the cytosolic Ca^{2+} transients at the two ages analysed (figure 4A). However, at the mitochondrial level, a decrease in basal Ca^{2+} was observed in brains from 21-day-old flies when compared with brains from younger (4-day-old) flies (figure 4B(i)). Moreover, the peak height was lower compared to 4-day-old flies (figure 4B(ii)), while the rate of Ca^{2+} uptake (first positive derivative) was decreased (figure 4B(iii)).

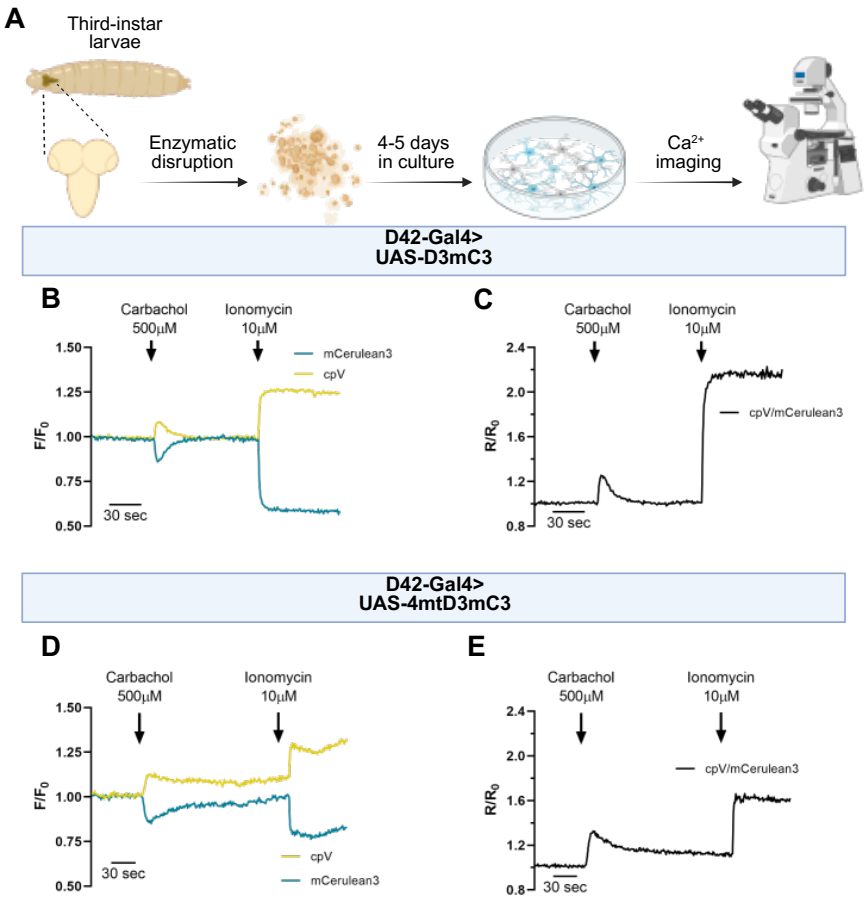

Figure 2. Ca^{2+} imaging in cultured neurons. (A) Schematic representation of the experimental design. Representative traces from each emission channel (mCerulean3 and cpV) recorded in motor neurons expressing D3mC3 (B) or 4mtD3mC3 (D) upon application of the indicated drugs. The fluorescence ratio (cpV/mCerulean3) is shown in (C,E), related to (B,D), respectively.

3.4. Ca^{2+} dynamics imaged by Cameleon probe in *Drosophila* heart

Imaging Ca^{2+} dynamics presents unique challenges in moving samples, such as beating cardiomyocytes, where cell contraction leads to an increase in the fluorescence of Ca^{2+} indicators independent of changes in [Ca^{2+}], thus resulting in potential overestimation of Ca^{2+} transients. This issue can be successfully addressed by using ratiometric sensors. Here, we tested the performance of the Cameleon sensor in measuring cytosolic Ca^{2+} transients during spontaneous heart beating in different experimental conditions: intact, live flies (figure 5A), semi-intact heart preparation (figure 5B), and isolated heart (figure 5C). Fourteen-day-old flies expressing UAS-D3mC3 under the control of the muscle-specific driver MHC-Gal4 were used. During cardiac contraction, the fluorescence measured upon emission of the two FPs increased due to sensor accumulation (figure 5D). However, this movement artefact was corrected by the calculation of the ratio of the two (figure 5D′). Additionally, a myosin ATPase inhibitor (BDM) was employed to suppress contraction by uncoupling actin–myosin interaction without interfering with Ca^{2+} handling. In the presence of BDM, we observed the expected antiparallel trend of the fluorescence emitted by the two FPs, which is indicative of the energy transfer from donor to acceptor (figure 5E) and the consequent R changes (figure 5E′). Maximal and minimal Ca^{2+} levels were achieved by applying ionomycin in the presence of Ca^{2+} (figure 5F), then EGTA (figure 5F′), respectively, in the presence of BDM.

4. Discussion

This study describes the generation and characterization of two innovative transgenic fly lines for the expression of cytosolic and mitochondria-targeted mCerulean3-based Cameleon probes for ratiometric Ca^{2+} imaging in *Drosophila melanogaster*. FRET-based sensors were chosen for their reliability in dynamic environments, like mitochondria, and moving samples, such as hearts, despite their narrower dynamic range compared to intensity-based probes like GCaMPs. Notably, the use of Cameleons incorporating mCerulean3 as the donor FP overcame some of the limitations associated with earlier versions of FRET donor ECFP, including pH sensitivity and low fluorescence quantum yield [15]. As a consequence, the sensors present negligible dependence of the ratio on pH variations, which could occur in various physiological or pathological conditions, particularly in the mitochondrial matrix [13]. Moreover, the significant increase in the signal-to-noise ratio provided by mCerulean3-based sensors makes these sensors an ideal choice for transgenic animal generation and visualization of small organelles like mitochondria.

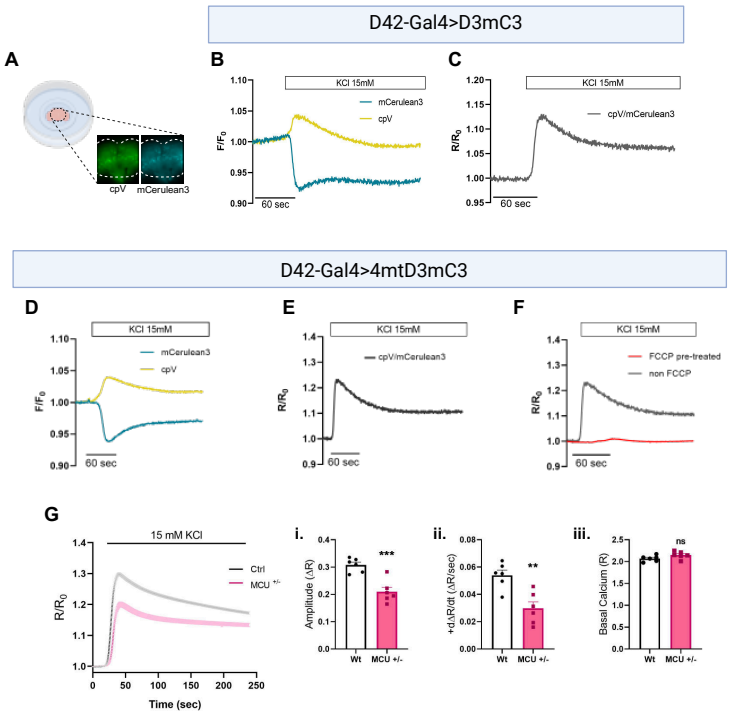

Figure 3. Ca^{2+} imaging of brains from three-week-old D42-Gal4 > UAS-D3mC3 or D42-Gal4 > UAS-4mtD3mC3 flies. (A) Schematic representation of the naked brain preparation and representative microscope images. (B) Representative traces of each wavelength (mCerulean3 and cpV) recorded in motor neurons expressing D3mC3 upon application of KCl. Data are plotted as F/F_0. (C) Representative kinetics of cytosolic Ca^{2+} dynamics in neurons expressing D3mC3 challenged with KCl. Data are plotted as R/R_0. (D) Representative traces of each emission channel (mCerulean3 and cpV) recorded in motor neurons expressing 4mtD3mC3 upon application of KCl. Data are plotted as F/F_0. (E) Representative kinetics of mitochondrial Ca^{2+} dynamics in neurons expressing 4mtD3mC3 challenged with KCl. Data are plotted as R/R_0. (F) Representative kinetics of mitochondrial Ca^{2+} dynamics in neurons expressing 4mtD3mC3 challenged with KCl in the presence (red) or not (grey) of the mitochondrial uncoupler FCCP. Data are plotted as R/R_0. (G) Average traces of R/R_0 from control and $MCU^{+/-}$ 4-day-old fly brains. Bar graphs showing the mean ± s.e.m. of peak height (i), rate of Ca^{2+} uptake (ii), and basal (iii) Ca^{2+} level. $n = 6$ brains per genotype (mean of at least 5 neurons per brain).

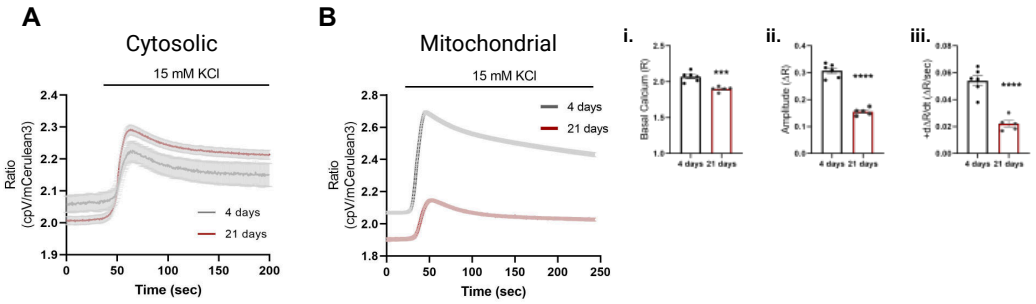

Figure 4. Ca^{2+} imaging in brains from D42-Gal4 > UAS-D3mC3 or D42-Gal4 > UAS-4mtD3mC3 flies at different ages. Representative traces of fluorescence ratio (cpV/mCerulean3) during KCl application, recorded in motor neurons expressing D3mC3+16 (A) or 4mtD3mC3+16 (B). Bar graphs showing the mean ± s.e.m. of the basal Ca^{2+} level (i), peak height (ii), and rate of Ca^{2+} uptake (iii). $n = 3$ and 5 brains per time point, cytosolic and mitochondrial, respectively (mean of at least 5 neurons per brain).

The study of Ca^{2+} dynamics in living organisms is still challenging, and quantitative measurements of mitochondrial matrix $[Ca^{2+}]$ often result in surprisingly different results [30]. The generation of sensors with diverse photophysical properties, such as different K_d, dynamic range and signal-to-noise ratio, is necessary to enhance our ability to observe the functionality of mitochondria in complex systems. Different imaging techniques benefit from sensors with specific properties. Intensiometric sensors with low baseline fluorescence are advantageous for imaging extensive cell populations in densely labelled samples, minimizing background signals. Conversely, organelles and cellular compartments, with their minute dimensions, pose challenges due to limited fluorescence and heightened susceptibility to photobleaching. In such scenarios, sensors with substantial baseline fluorescence are preferred. Moreover, high baseline fluorescence proves beneficial for imaging sparsely labelled samples.

Our investigation focused on two critical organs where Ca^{2+} regulation is crucial: the brain and the heart. It has been reported that *Drosophila* presynaptic neurons exhibit a resting mitochondrial $[Ca^{2+}]$ of approximately 0.2 µM, which rises to

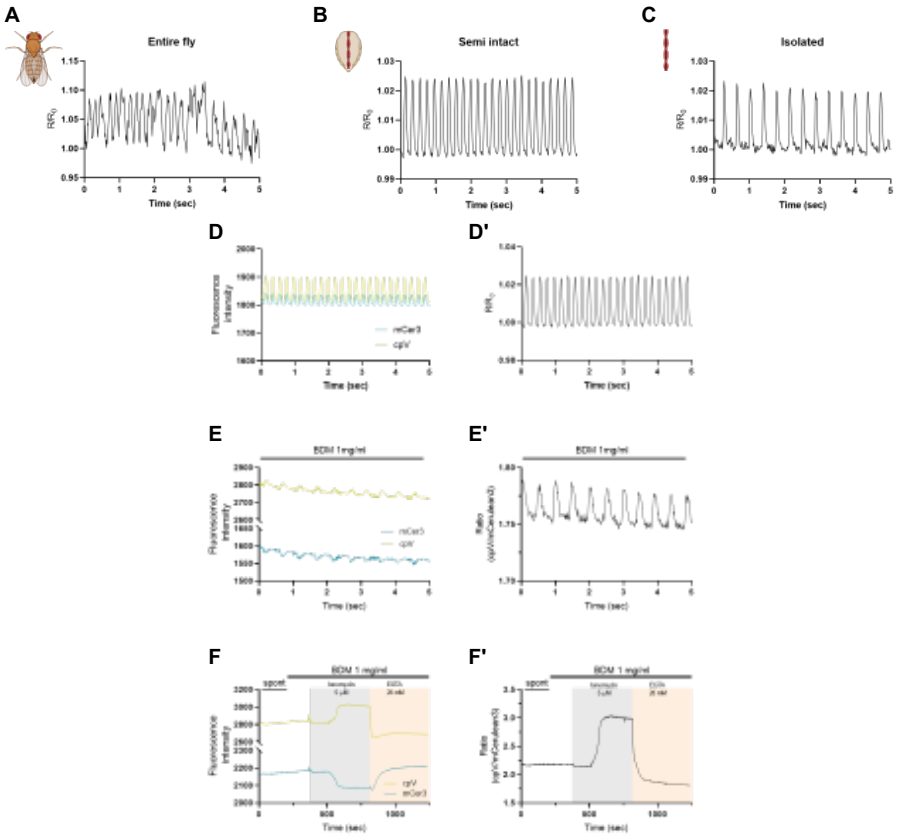

Figure 5. Ca^{2+} imaging in 14-day-old hearts from MHC-Gal4 > UAS-D3mC3 flies. (A–C) Representative traces of fluorescence ratio (cpV/mCerulean3) during spontaneous heart beating in the live fly (A), semi-intact heart preparation (B) and isolated heart (C). (D–F′) Representative traces from each emission channel (mCerulean3 and cpV, left) or of the ratio (right) recorded in semi-intact hearts (as in B) expressing D3mC3 during spontaneous heart beating in the absence (D,D′) or presence (E,E′) of BDM. (F,F′) Maximal and minimal Ca^{2+} levels were achieved by applying 5 µM ionomycin and 20 mM EGTA, respectively, in the presence of BDM, after recording spontaneous beating (spont).

about 27.0 µM upon axon firing [13]. On the other hand, quantitative mitochondrial [Ca^{2+}] measurements in cardiomyocytes of fruit flies have not been thoroughly explored. For the generation of the new Cameleon fly lines, we selected D3 variants for their suitability for experimental needs regarding Ca^{2+} affinity. Indeed, similar to the original D3-based Cameleon, the mCerulean3-based probe maintains a single K_d for Ca^{2+}, sensing [Ca^{2+}] (K_d D3mC3+16 ≈ 4.1 µM at pH 7; K_d 4mtD3mC3+16 ≈ 6.2 µM at pH 8 [15]), placing it in a suitable range for both resting and stimulated [Ca^{2+}] measurements.

The expression of these probes in specific cell types was achieved using the UAS/Gal4 system, enabling precise spatial control and avoiding potential toxicity from constitutive expression. Although the cytosolic probe did not adversely affect fly survival, the construct targeted to mitochondria resulted in lethality under certain drivers, such as tubulin-Gal4, daughterless-Gal4, and the muscular driver Mef2-Gal4. To mitigate lethality, weaker drivers like MHC-Gal4 were necessary. The exact cause of the observed lethality remains unclear. Typically, the presence of Ca^{2+} sensors can impact survival due to their buffering capacity. However, the probes used possess a K_d in the micromolar range, indicating limited Ca^{2+} buffering capacity at baseline. Instead, the larger size of FRET sensors, compared to single-wavelength probes, might disturb mitochondrial physiology when the probes are confined in the mitochondrial matrix, particularly in tissues characterized by mitochondria with small matrix space. This might trigger toxicity, particularly in tissue areas highly dependent on mitochondrial function. Therefore, regulated expression of Ca^{2+} sensors, both temporally and spatially, is preferred over constitutive expression to prevent disruption of cellular physiology, which heavily relies on proper mitochondrial function.

By crossing D42-Gal4 with UAS-4mtD3mC3 or UAS-D3mC3, we expressed the probes in motor neurons to assess their functionality in both isolated cells and tissue preparations, demonstrating their efficacy in detecting Ca^{2+} transients in various experimental paradigms. In cultured neurons, both cytosolic and mitochondria-targeted probes accurately reported changes in Ca^{2+} levels in response to pharmacological stimuli, with comparable performance observed between the two probes. Similar results were obtained in adult brain preparations, confirming the probes' utility in *ex vivo* settings. Furthermore, the mitochondrial probe's capability to report changes in [Ca^{2+}] within the mitochondrial matrix is confirmed by the abolishment of mitochondrial Ca^{2+} uptake upon mitochondrial membrane potential dissipation. Additionally, we leveraged a known paradigm capable of reducing mitochondrial Ca^{2+} uptake: the modulation of MCU expression. Under a partial reduction of the MCU in young flies, a reduction in mitochondrial Ca^{2+} uptake upon KCl stimulation (peak height and first derivative) was observed without changes in basal levels. These data are in agreement with previous reports [11,31] and further validate the suitability of the new fly line to measure mitochondrial Ca^{2+} dynamics.

Mitochondrial Ca^{2+} mishandling has been observed in the ageing brain and neurodegenerative diseases [32]. Effective tools are crucial for studying these processes comprehensively in animal models, especially for investigating Ca^{2+} dynamics across

an individual's lifespan. Here, we compared mitochondrial Ca^{2+} dynamics in young versus old flies, uncovering changes in basal Ca^{2+} levels and uptake kinetics during ageing. Specifically, older flies displayed reduced basal mitochondrial [Ca^{2+}], along with diminished Ca^{2+} uptake upon KCl stimulation, when compared to their younger counterparts. These findings align with previous observations in mammalian models [33–36] and foster the use of *Drosophila* as a model for Ca^{2+} imaging when studying age-associated and neurodegenerative conditions. Notably, the ability of the probe to detect basal mitochondrial [Ca^{2+}] variations highlights its suitability for detecting baseline changes in mitochondrial [Ca^{2+}].

Ratiometric imaging with the cytosolic Cameleon sensor enabled us to precisely monitor Ca^{2+} transients in cardiac tissue, overcoming challenges posed by sample movement during heartbeating. Importantly, we were able to monitor cytosolic [Ca^{2+}] variations in semi-intact heart preparations and isolated hearts, as well as in the intact awake fly. The latter offers the possibility to get insights into Ca^{2+} dynamics during cardiac contraction while only minimally impacting fly physiology.

This study establishes an approach to measure cardiac Ca^{2+} dynamics in an entire living fly. This approach offers the possibility of studying cardiac Ca^{2+} handling in a physiological context and also enables investigation of organ cross-talk, such as brain–heart communication.

In conclusion, our study introduces novel transgenic fly lines expressing cytosolic and mitochondria-targeted mCerulean3-based Cameleon probes, providing reliable tools for investigating mitochondrial and cytosolic Ca^{2+} dynamics in *Drosophila melanogaster*. These tools will broaden our ability to explore cytosolic and mitochondrial Ca^{2+} dynamics *in vivo* in the simple model *Drosophila melanogaster*, which offers easier handling and less labour-intensive imaging preparation procedures compared to mammalian models.

Ethics. This work did not require ethical approval from a human subject or animal welfare committee.

Data accessibility. The data from this article have been made publicly available in the Zenodo repository [37]. DNA sequences and raw western blot images are available as electronic supplementary material [38].

Declaration of AI use. We have not used AI-assisted technologies in creating this article.

Authors' contributions. M.S.: conceptualization, formal analysis, investigation, methodology, visualization, writing—review and editing; S.S.: investigation, methodology, visualization, writing—review and editing; A.B.: investigation, methodology, writing—review and editing; A.C.P.: writing—review and editing; E.G.: conceptualization, methodology, project administration, writing—review and editing; D.P.: conceptualization, funding acquisition, methodology, project administration, resources, writing—original draft, writing—review and editing.

All authors gave final approval for publication and agreed to be held accountable for the work performed therein.

Conflict of interest declaration. We declare we have no competing interests.

Funding. This research was funded by Fondazione Cassa di Risparmio di Padova e Rovigo (CARIPARO) Starting Grant 2015, Fondazione Telethon (GGP19304) and Fondazione Cariplo/Fondazione Telethon (GJC21054) to D.P.; European Union's Horizon Europe research and innovation programme under Marie Skłodowska-Curie grant agreement no. 101109589 to M.S. and D.P. The imaging instruments used were available thanks to UNIPD Funds for Research Equipment-2015; Euro-BioImaging FOE (MUR); National Recovery and Resilience Plan (NRRP), Mission 4 Component 2 Investment 3.1-Call for tender no. 3264/2021 of Italian MUR, funded by the European Union–NextGenerationEU, Project code IR0000023, Concession Decree No. 101/2022 adopted by the Italian MUR, CUP B53C22001810006, 'SEELIFE—Strengthening the Italian Infrastructure of Euro-Bioimaging'.

Acknowledgements. We thank José Duhart for helpful suggestions, Gloria Martignago for the help in Ca^{2+} imaging experiments of cultured neurons and Nicola Vajente for the help with fly husbandry and Ca^{2+} imaging experiments of cultured neurons. *MCU*^{1} fly line was kindly gifted by Alex Whitworth. Figures were created with BioRender.com.

References

1. Vajente N, Norante R, Pizzo P, Pendin D. 2020 Calcium imaging in *Drosophila melanogaster*. In *Calcium signaling* (ed. M Islam), pp. 881–900. Cham, Switzerland: Springer. (doi:10.1007/978-3-030-12457-1_35)
2. Redolfi N, García-Casas P, Fornetto C, Sonda S, Pizzo P, Pendin D. 2021 Lighting up Ca^{2+} dynamics in animal models. *Cells* **10**, 2133. (doi:10.3390/cells10082133)
3. Ugur B *et al*. 2017 The Krebs cycle enzyme isocitrate dehydrogenase 3A couples mitochondrial metabolism to synaptic transmission. *Cell Rep.* **21**, 3794–3806. (doi:10.1016/j.celrep.2017.12.005)
4. Fiala A, Spall T, Diegelmann S, Eisermann B, Sachse S, Devaud JM, Buchner E, Galizia CG. 2002 Genetically expressed cameleon in *Drosophila melanogaster* is used to visualize olfactory information in projection neurons. *Curr. Biol.* **12**, 1877–1884. (doi:10.1016/s0960-9822(02)01239-3)
5. Fiala A, Spall T. 2003 In vivo calcium imaging of brain activity in *Drosophila* by transgenic cameleon expression. *Sci. STKE* **2003**, pl6. (doi:10.1126/stke.2003.174.pl6)
6. Diegelmann S, Fiala A, Leibold C, Spall T, Buchner E. 2002 Transgenic flies expressing the fluorescence calcium sensor cameleon 2.1 under UAS control. *Genesis* **34**, 95–98. (doi:10.1002/gene.10112)
7. Inoshita T, Imai Y. 2021 Cytosolic and mitochondrial Ca^{2+} imaging in *Drosophila* dopaminergic neurons. In *Experimental models of Parkinson's disease* (ed. Y Imai), pp. 207–214. New York, NY: Springer. (doi:10.1007/978-1-0716-1495-2_20)
8. Terhzaz S, Southall TD, Lilley KS, Kean L, Allan AK, Davies SA, Dow JAT. 2006 Differential gel electrophoresis and transgenic mitochondrial calcium reporters demonstrate spatiotemporal filtering in calcium control of mitochondria. *J. Biol. Chem.* **281**, 18849–18858. (doi:10.1074/jbc.M603002200)
9. Lutas A, Wahlmark CJ, Acharjee S, Kawasaki F. 2012 Genetic analysis in *Drosophila* reveals a role for the mitochondrial protein P32 in synaptic transmission. *G3* **2**, 59–69. (doi:10.1534/g3.111.001586)
10. Imai Y, Inoshita T, Meng H, Shiba-Fukushima K, Hara KY, Sawamura N, Hattori N. 2019 Light-driven activation of mitochondrial proton-motive force improves motor behaviors in a *Drosophila* model of Parkinson's disease. *Commun. Biol.* **2**, 424. (doi:10.1038/s42003-019-0674-1)
11. Drago I, Davis RL. 2016 Inhibiting the mitochondrial calcium uniporter during development impairs memory in adult *Drosophila*. *Cell Rep.* **16**, 2763–2776. (doi:10.1016/j.celrep.2016.08.017)
12. Serrat R, Oliveira-Pinto A, Marsicano G, Pouvreau S. 2022 Imaging mitochondrial calcium dynamics in the central nervous system. *J. Neurosci. Methods* **373**, 109560. (doi:10.1016/j.jneumeth.2022.109560)

13. Ivannikov MV, Macleod GT. 2013 Mitochondrial free Ca^{2+} levels and their effects on energy metabolism in *Drosophila* motor nerve terminals. *Biophys. J.* **104**, 2353–2361. (doi:10.1016/j.bpj.2013.03.064)
14. Chouhan AK, Zhang J, Zinsmaier KE, Macleod GT. 2010 Presynaptic mitochondria in functionally different motor neurons exhibit similar affinities for Ca^{2+} but exert little influence as Ca^{2+} buffers at nerve firing rates in situ. *J. Neurosci.* **30**, 1869–1881. (doi:10.1523/JNEUROSCI.4701-09.2010)
15. Greotti E *et al*. 2019 mCerulean3-based cameleon sensor to explore mitochondrial Ca^{2+} dynamics in vivo. *iScience* **16**, 340–355. (doi:10.1016/j.isci.2019.05.031)
16. Brand AH, Perrimon N. 1993 Targeted gene expression as a means of altering cell fates and generating dominant phenotypes. *Development* **118**, 401–415. (doi:10.1242/dev.118.2.401)
17. Tufi R, Gleeson TP, von Stockum S, Hewitt VL, Lee JJ, Terriente-Felix A, Sanchez-Martinez A, Ziviani E, Whitworth AJ. 2019 Comprehensive genetic characterization of mitochondrial Ca^{2+} uniporter components reveals their different physiological requirements *in vivo*. *Cell Rep.* **27**, 1541–1550.(doi:10.1016/j.celrep.2019.04.033)
18. Vajente N, Norante R, Redolfi N, Daga A, Pizzo P, Pendin D. 2019 Microtubules stabilization by mutant spastin affects er morphology and Ca^{2+} handling. *Front. Physiol.* **10**, 1544. (doi:10.3389/fphys.2019.01544)
19. Duhart JM, Herrero A, de la Cruz G, Ispizua JI, Pírez N, Ceriani MF. 2020 Circadian structural plasticity drives remodeling of E cell output. *Curr. Biol.* **30**, 5040–5048. (doi:10.1016/j.cub.2020.09.057)
20. Vogler G, Ocorr K. 2009 Visualizing the beating heart in *Drosophila*. *J. Vis. Exp* **31**, e1425. (doi:10.3791/1425)
21. Santalla M, García A, Mattiazzi A, Valverde CA, Schiemann R, Paululat A, Hernández G, Meyer H, Ferrero P. 2022 Interplay between SERCA, 4E-BP, and eIF4E in the *Drosophila* heart. *PLoS One* **17**, e0267156. (doi:10.1371/journal.pone.0267156)
22. Palmer AE, Giacomello M, Kortemme T, Hires SA, Lev-Ram V, Baker D, Tsien RY. 2006 Ca^{2+} indicators based on computationally redesigned calmodulin-peptide pairs. *Chem. Biol.* **13**, 521–530. (doi:10.1016/j.chembiol.2006.03.007)
23. De Stefani D, Raffaello A, Teardo E, Szabò I, Rizzuto R. 2011 A forty-kilodalton protein of the inner membrane is the mitochondrial calcium uniporter. *Nature* **476**, 336–340. (doi:10.1038/nature10230)
24. Baughman JM *et al*. 2011 Integrative genomics identifies MCU as an essential component of the mitochondrial calcium uniporter. *Nature* **476**, 341–345. (doi:10.1038/nature10234)
25. Martin N, Bernard D. 2018 Calcium signaling and cellular senescence. *Cell Calcium* **70**, 16–23. (doi:10.1016/j.ceca.2017.04.001)
26. Arjun McKinney A, Petrova R, Panagiotakos G. 2022 Calcium and activity-dependent signaling in the developing cerebral cortex. *Development* **149**, dev198853. (doi:10.1242/dev.198853)
27. Stewart TA, Davis FM. 2019 An element for development: calcium signaling in mammalian reproduction and development. *Biochim. Biophys. Acta Mol. Cell Res.* **1866**, 1230–1238. (doi:10.1016/j.bbamcr.2019.02.016)
28. Zarate SM, Huntington TE, Bagher P, Srinivasan R. 2023 Aging reduces calreticulin expression and alters spontaneous calcium signals in astrocytic endfeet of the mouse dorsolateral striatum. *npj Aging* **9**, 5. (doi:10.1038/s41514-023-00102-8)
29. Leclerc C, Moreau M, Néant I. 2012 The calcium: an early signal that initiates the formation of the nervous system during embryogenesis. *Front. Mol. Neurosci.* **5**, 3. (doi:10.3389/fnmol.2012.00064)
30. Fernandez-Sanz C, De la Fuente S, Sheu SS. 2019 Mitochondrial Ca^{2+} concentrations in live cells: quantification methods and discrepancies. *FEBS Lett.* **593**, 1528–1541. (doi:10.1002/1873-3468.13427)
31. Twyning MJ *et al*. 2024 Partial loss of MCU mitigates pathology in vivo across a diverse range of neurodegenerative disease models. *Cell Rep.* **43**, 113681. (doi:10.1016/j.celrep.2024.113681)
32. Phillips MCL, Picard M. 2024 Neurodegenerative disorders, metabolic icebergs, and mitohormesis. *Transl. Neurodegener.* **13**, 46. (doi:10.1186/s40035-024-00435-8)
33. Xiong J, Verkhratsky A, Toescu EC. 2002 Changes in mitochondrial status associated with altered Ca^{2+} homeostasis in aged cerebellar granule neurons in brain slices. *J. Neurosci.* **22**, 10761–10771. (doi:10.1523/JNEUROSCI.22-24-10761.2002)
34. Pandya JD, Grondin R, Yonutas HM, Haghnazar H, Gash DM, Zhang Z, Sullivan PG. 2015 Decreased mitochondrial bioenergetics and calcium buffering capacity in the basal ganglia correlates with motor deficits in a nonhuman primate model of aging. *Neurobiol. Aging* **36**, 1903–1913. (doi:10.1016/j.neurobiolaging.2015.01.018)
35. Müller M, Ahumada-Castro U, Sanhueza M, Gonzalez-Billault C, Court FA, Cárdenas C. 2018 Mitochondria and calcium regulation as basis of neurodegeneration associated with aging. *Front. Neurosci.* **12**, 470. (doi:10.3389/fnins.2018.00470)
36. Murchison D, Zawieja DC, Griffith WH. 2004 Reduced mitochondrial buffering of voltage-gated calcium influx in aged rat basal forebrain neurons. *Cell Calcium* **36**, 61–75. (doi:10.1016/j.ceca.2003.11.010)
37. Santalla M, Sonda S, Bertocco A, Ciocci Pardo A, Greotti E, Pendin D. 2025 FRET-based fluorescent sensors for cytosolic and mitochondrial Ca^{2+} imaging in *Drosophila melanogaster* [Data set]. Zenodo. (doi:10.5281/zenodo.17285210)
38. Santalla M, Sonda S, Bertocco A, Ciocci Pardo A, Greotti E, Pendin D. 2026 Supplementary material from: FRET-based Fluorescent Sensors for Cytosolic and Mitochondrial Ca^{2+} Imaging in *Drosophila melanogaster*. Figshare (doi:10.6084/m9.figshare.c.8254418)